Heliyon 10 (2024) e24962

Contents lists available at ScienceDirect

Heliyon

journal homepage: www.cell.com/heliyon

Research article

Cholangiocyte-derived exosomal long noncoding RNA PICALM-AU1 promotes pulmonary endothelial cell endothelial-mesenchymal transition in hepatopulmonary syndrome

Congwen Yang [a,b], Yihui Yang [c], Yang Chen [a], Jian Huang [a], Dan Li [a], Xi Tang [a], Jiaolin Ning [a], Jianteng Gu [a], Bin Yi [a,**], Kaizhi Lu [a,*]

[a] Department of Anesthesia, Southwest Hospital, The Third Military Medical University, Chongqing 400038, China
[b] Chongqing Key Laboratory of Traditional Chinese Medicine for Prevention and Cure of Metabolic Diseases, Chongqing Medical University, Chongqing, 400016, China
[c] Department of Anesthesia, The Third Affiliated Hospital of Zunyi Medical University, Zunyi, Guizhou, 563000 China

ARTICLE INFO

Keywords:
Long noncoding RNA (lncRNA)
PICALM-AU1
Endothelial-mesenchymal transition (EndMT)
Hepatopulmonary syndrome

ABSTRACT

Hepatopulmonary syndrome (HPS) is a severe lung injury caused by chronic liver disease, with limited understanding of the disease pathology. Exosomes are important mediators of intercellular communication that modulates various cellular functions by transferring a variety of intracellular components to target cells. Our recent studies have indicated that a new long noncoding RNA (lncRNA), PICALM-AU1, is mainly expressed in cholangiocytes, and is dramatically induced in the liver during HPS. However, the mechanism by which cholangiocyte-derived PICALM-AU1 regulates Endothelial-mesenchymal transition (EndMT) in HPS remains unclear. Here, we observed that PICALM-AU1 was synthesized in the cholangiocytes of the liver and then, secreted as exosomes into the serum; serum exosomal PICALM-AU1 levels were positively correlated with the severity of HPS in a rat model and in human patients. PICALM-AU1 carrying serum exosomes induced the EndMT of pulmonary microvascular endothelial cells (PMVECs) and promoted lung injury in vivo and in vitro. Furthermore, PICALM-AU1 acted as a molecular sponge for microRNA 144-3p (miR144-3p), resulting in the up-regulation of Zinc Finger E-Box Binding Homeobox 1 (ZEB1), a known target of EndMT and enhancement of EndMT, proliferation and migration of PMVECs. Taken together, our findings indicate that the cholangiocyte-derived exosomal lncRNA PICALM-AU1 plays a critical role in the EndMT in HPS lungs. Thus, it represents a potential therapeutic target for the treatment of HPS.

1. Introduction

Hepatopulmonary syndrome (HPS), characterized by hypoxemia and intrapulmonary shunting, occurs in 5–32 % of patients with liver disease [1]; It significantly increases mortality and worsens the functional status and quality of life in patients with cirrhosis [2].

* Corresponding author.
** Corresponding author.
E-mail addresses: yibin@tmmu.edu.cn (B. Yi), lukaizhi@tmmu.edu.cn (K. Lu).

https://doi.org/10.1016/j.heliyon.2024.e24962
Received 28 June 2023; Received in revised form 15 January 2024; Accepted 17 January 2024
Available online 18 January 2024

Despite increasing knowledge of the mechanisms involved in HPS development, its pathogenesis has not been fully unraveled [3–5].

Pulmonary angiogenesis plays a vital role in developing HPS [6]. Soluble molecules synthesized in pathological liver, such as the vascular endothelial growth factor (VEGF), bone morphogenic protein-2 (BMP2), BMP9, and placental growth factor (PIGF), act as pro-angiogenic factors and are transported into the lungs, where they induce gene expression and promote pulmonary microvascular formation, thus aggravating the degree of respiratory distress in HPS [7–10]. Endothelial-mesenchymal transition (EndMT) is a process that is characterized by the loss of endothelial cell features and the acquisition of specific markers of mesenchymal cells, which plays a key role in regulating endothelial function, development and structural remodeling of the myocardium, blood vessels, and valves [11–13]. Numbers studies have implicated EndMT in the vascular diseases, including cerebral cavernous malformations, pulmonary hypertension, vascular graft remodeling, tumorigenesis, and atherosclerosis [14–18]. Chronic obstructive lung disease (COPD) is caused by hypoxia or other hypoxia-independent stimuli-induced pulmonary vascular remodeling. The expression of S100A4 expression was observed in the remodeled intrapulmonary arteries of patients with COPD, suggesting that S100A4 could serve as a potential therapeutic target for preventing vascular remodeling in patients with COPD [19,20]. However, the mechanism by which EndMT regulates HPS pathology is largely unclear, although recent studies have indicated possible links between EndMT and exosomes [21].

Exosomes, are small extracellular membrane-enclosed vesicles formed by the inward budding of endosomal members and released extracellularly via fusion with the plasma membrane. Exosomal cargos, including noncoding RNAs, proteins, and lipids, are implicated in various diseases [22–25]. The cholangiocyte-derived exosomal LncRNA H19 promotes hepatic stellate cell activation and cholestatic liver fibrosis [26,27]. In our previous study, we reported that hepatocyte-derived exosomal miR 194 promotes pulmonary microvascular endothelial cell (PMVECs) angiogenesis in HPS pulmonary tissue [28]. This study preliminarily described that in HPS, exosomes secreted into the serum promoted pulmonary microvessels formation. However, apart from microRNAs, lncRNAs in exosomes play important regulatory roles in physiological functions and pathological processes. We aimed to explore whether exosomes synthesized from the liver contained potentially important lncRNAs, and to control HPS pathology through a long-distance regulation mechanism across organs.

In this study, a novel lncRNA (MRAK138283, named PICALM-AU1) was identified by microarray screening of the HPS rat liver. We demonstrated that PICALM-AU1 is rich in cholangiocyte-derived exosomes from the HPS rat liver. The quantity of PICALM-AU1 in serum exosomes is positively correlated with the severity of lung injury in rat HPS models and human HPS patients. We observed that the cholangiocyte-derived exosome PICALM-AU1 is a key molecule that promotes the EndMT of PMVECs in HPS. This suggests that the exosome-derived lncRNA PICALM-AU1 from the HPS liver regulates lung injury. Thus, PICALM-AU1 may be a potential therapeutic target for HPS.

2. Materials and methods

2.1. Animal model and treatments

Common bile duct ligation rat model (CBDL). The common bile duct ligation operation in rat is a well-established model for studying HPS [28,29]. All animal experiments were approved by the Animal Care Committee of Third Military Medical University, Chongqing, China. Male Sprague-Dawley rats weighing 200–220 g and aged 6–7 weeks were used, with 30 rats in each group. The rats were anesthetized with intramuscular injections of ketamine (80 mg/kg) and xylazine (10 mg/kg). The control group underwent a sham-operation in which the common bile duct was isolated without ligation. The lung tissue of the rats was dissected and analyzed at 1 week, 3 weeks and 5 weeks after surgery. Blood samples were aseptically drawn from the abdominal aorta during laparotomy. A 0.2 ml sample of arterial blood was collected in a heparinized gas capillary tube to measure the arterial gas levels. Serum was separated from the blood samples by centrifugation at 2000×*g* and 4 °C, and then used to isolate exosomes.

Arterial blood gas analysis and sample preparation. Arterial blood was collected from the abdominal aorta under chloral hydrate anesthesia (40 mg/kg IP, Nembutal, Ceva Sante Animale). The blood gas analysis was performed at the Laboratory of Clinical Biology in Southwest Hospital, China. Hypoxemia was defined as a $PaO_2 < 80$ mmHg. Serum was prepared by centrifuging the blood at 10,000 rpm for 10 min at 4 °C and stored at −80 °C before analysis.

Exosome treatment. To analyze the function of HPS exosomes on rat lungs, exosomes isolated from sham rat serum, HPS rat serum, MIBECs cell line and MIBECs with PICALM-AU1 overexpression were injected into healthy rats (200–220 g, 6–7 weeks old). The rats were randomly divided into four groups: ss-Exo (sham-serum exosome); Hs-Exo (HPS serum exosome); ct-Exo (MIBECs-derived exosome); PO-Exo (PICALM-AU1 OE MIBECs-derived exosome). Each group received three injections of exosomes (100 μg total protein in 100 μL volume) via the caudal vein with one injection given every other day. Exosomes from sham and HPS rat serum were also used to treat PMVECs in order to analyze EndMT in the cell line.

Virus treatment. To analyze the function of PICALM-AU1 on rat lungs, lentivirus with PICALM-AU1 overexpression and knockdown was constructed. The LV-NC, LV-PICALM-OE and LV-PICALM-KD viruses were injected into healthy rats (200–220 g, 6–7 weeks age) via caudal vein (each at 100 μL of 2×10^{10} TU/ml). After two weeks, the rats were carried on CBDL operation; To investigate the function of exosomal-PICALM-AU1 toward rat lung, lentivirus LV-NC and LV-PICALM-OE were treated MIBECs (each at 10 μL of 1×10^9 TU/mL). After 72 h, detection of the PICALM-AU1 expression. And then, exosome was isolated for rat infection; To analysis the function of PICALM-AU1 toward PMVECs, LV-NC, LV-PICALM-OE and LV-PICALM-KD viruses were treated PMVECs (each at 10 μL of 1×10^9 TU/mL). After 72 h, detection of the gene expression, protein synthesis was carried on.

2.2. Microarray analysis

Total RNA of CBDL operation group and sham group rat liver was extracted and transcribed. Double-stranded cDNA was labeled using the Quick Amp Labeling Kit (Agilent Technologies Inc, USA) and hybridized to the Array star Rat 8 × 60 K lncRNA Array, version 2.0. Following the washing steps, the arrays were scanned with the Agilent Scanner G2505B, and the array images were analyzed using Agilent Feature Extraction software, version 10.7.3.1. Quantile normalization and subsequent data processing were performed using GeneSpring GX software, version 11.5.1 (Agilent Technologies Inc, USA). Volcano plot filtering was used to identify the lncRNAs with statistically significant differences, and the threshold to screen upregulated or downregulated lncRNAs was identified at a fold change of 1.5 or greater and a P value of 0.05 or less.

2.3. Tissue harvest and histology

Liver and lung samples were fixed in a 4 % phosphate buffered formaldehyde solution (Klinipath, Belgium). They were then dehydrated, embedded in paraffin, and subjected to various staining techniques including Hematoxylin and eosin, Masson, Immunohistochemistry, Immunofluorescence and Fluorescence *in situ* hybridization. The antibody information for all the samples can be found in Table S2.

Hematoxylin and eosin staining of rat lung tissue was performed following a previous study [28]. Immunohistochemical staining was used to quantify protein expression levels in the lung tissue. Specific antibodies against VWF, VE-cadherin and Vimentin were utilized. Negative controls were included by omitting the primary antibodies or using IgG. The lung sections (5 μm thickness) embedded in paraffin were deparaffinized, rehydrated with ethanol, and pretreated with citrate buffer. Non-specific binding sites were blocked using 3 % H_2O_2 (Merck, Germany) and BSA. Epitope detection was carried out using the ultraView Universal DAB Detection Kit (Dako, Denmark). Hematoxylin was used for counterstaining.

The vascular density of specimens stained for VWF was measured semi-quantitatively using Cell Software (Olympus, Japan). The results are expressed as mean positively stained per field. The number of vascular structures per high power field (objective 40 ×) was counted in 15 randomly selected fields for each rat, and the mean value of the vascular structures in these fields was calculated (mean number of vascular structures per field ± SE). All final histological scores are represented as the mean of the scores determined by two independent researchers, who were blinded to the study samples.

Immunofluorescence. Paraffin-embedded lung sections (5 μm thickness) or cell slides were deparaffinized, rehydrated by serial immersion in ethanol and pretreated with EDTA. This was followed by incubation in 50 mM NH_4Cl, 0.1 % Triton X-100 and 1 % BSA. Primary antibodies used were anti-VE-cadherin, anti-Vimentin, anti-ZEB1 and anti-ZO1. Slices that underwent immunostaining with omission of primary antibodies or with IgG were used as negative controls. The binding sites of the primary antibodies were revealed with Alexa Fluor-594 goat anti-rabbit and Alexa Fluor-488 goat anti-mouse secondary antibodies (Invitrogen, USA). Nuclei were stained with 4′, 6-diamidino-2-phenylindole (DAPI) (Life Technologies, USA). Samples were visualized with a fluorescence microscope (Olympus, Japan).

FISH (Fluorescence in situ hybridization) combined with fluorescent IHC staining was performed on rat liver tissue sections targeting PICALM-AU1. This was done using a commercially available RNA scope Multiplex Fluorescent Reagent Kit v2 (Advanced Cell Diagnostics, USA) following the manufacturer's instruction. Fluorescent IHC staining targeting PICALM-AU1 was performed after FISH staining as described in the previous section (Histopathology, Masson's Trichrome staining, and immunohistochemistry). FISH results were visualized using Zeiss LSM 700 confocal laser scanning microscopy (Carl Zeiss, Germany).

2.4. cDNA synthesis and qPCR

The expression of LncRNA, miRNA and mRNA were analyzed in tissue and cell samples using the Applied Biosystems 7000 sequence detection system (Applied Biosystems, UK) with SYBR Green and the comparative CT method. The values were reported relative to the endogenous control glyceraldehyde-3-phosphate dehydrogenase. All amplification reactions were performed three times independently. The primer sequences were described in Supplementary Table S1.

2.5. Western blot

Protein expression was determined by Western blot in rat lung and PMVECs samples as previously described [30]. Antibody information can be found in Table S2. Blots were visualized using ECL reagents (DAKO, Denmark), and digital images were taken using a luminescent image analyzer LAS-4000 (General Electric, UK). β-actin was used for the normalization of quantitative densitometry values.

2.6. Cell culture and in vitro experiments

Rat pulmonary microvascular endothelial cells (PMVECs) and mouse intrahepatic biliary epithelial cells (MIBECs) were purchased from the American Type Culture Collection (ATCC Cell, VA, USA). Cells were maintained at 37 °C in RPMI medium (Gibco, USA) supplemented with 10 % fetal bovine serum (Invitrogen, USA). For cell transfection experiments, the cells were seeded at 60–70 % confluence. The vectors were mixed with Lipofectamine 3000 (Promega, USA), diluted in EGM2, and treated for 24 h, as described previously [30]. After 24 h, cells were treated with microRNA (miR144-3p) mimics/inhibitors or sham/HPS exosomes. Luciferase

(Luc) activity was detected by Dual-Luciferase Reporter Assay System (Promega, Madison, USA) in the GloMax-Multi Detection System Photometer (Promega). Assays were carried out three times independently and the average Luc activity levels were represented as means ± standard errors (SE).

2.7. Hepatopulmonary syndrome patient specimens

We selected patients with HPS and collected their blood sample. Exosomes were isolated to detect the gene transcripts. The study was approved by the ethics committee of human Care Committee of Third Military Medical University (No.2017 scientific research (35)) and the U.S. National Library of Medicine Clinical Trails (https://clinicaltrials.gov/, NCT:03435406). All participants provided written informed consent and agreed to the publication of their anonymous information. Inclusion criteria, 18–80 years old, American association of anesthesiologists (ASA) score: I-III; Ability to comply with research programs; Voluntary participation in the study; Has the history of HBV infection; No primary cardiopulmonary disease (heart disease, emphysema, pneumonia, asthma, etc). And exclusion criteria: severe heart, lung, kidney disease coexisted; American association of anesthesiologists (ASA) score ≥ IV; forced expiratory volume at 1 s (FEV1) or forced vital capacity (FVC) < 70 %, or FEV1/FVC <0.70; mental state could not cooperate; Absence of written informed consent. The patients were screened for HPS, which was diagnosed based on three parameters: (1) the presence of cirrhosis; (2) positive contrast-enhanced echocardiography; and (3) an alveolar-arterial oxygen gradient (P(A-a) O_2) ≥ 15 mmHg (or ≥20 mmHg in patients >64 years). Intrapulmonary vascular dilation was assessed using contrast-enhanced echocardiography. Agitated saline causes microbubbles of >10 μm in diameter that usually do not pass through the pulmonary capillary bed. The appearance of microbubbles, after injection in a peripheral vein, first in the right heart, and within three to six heart actions in the left heart demonstrates abnormal vasodilation of the intrapulmonary capillary bed. The early appearance (<3 heart beats) appearance of microbubbles in the left heart was considered as intracardiac shunting. These patients were excluded because the presence or absence

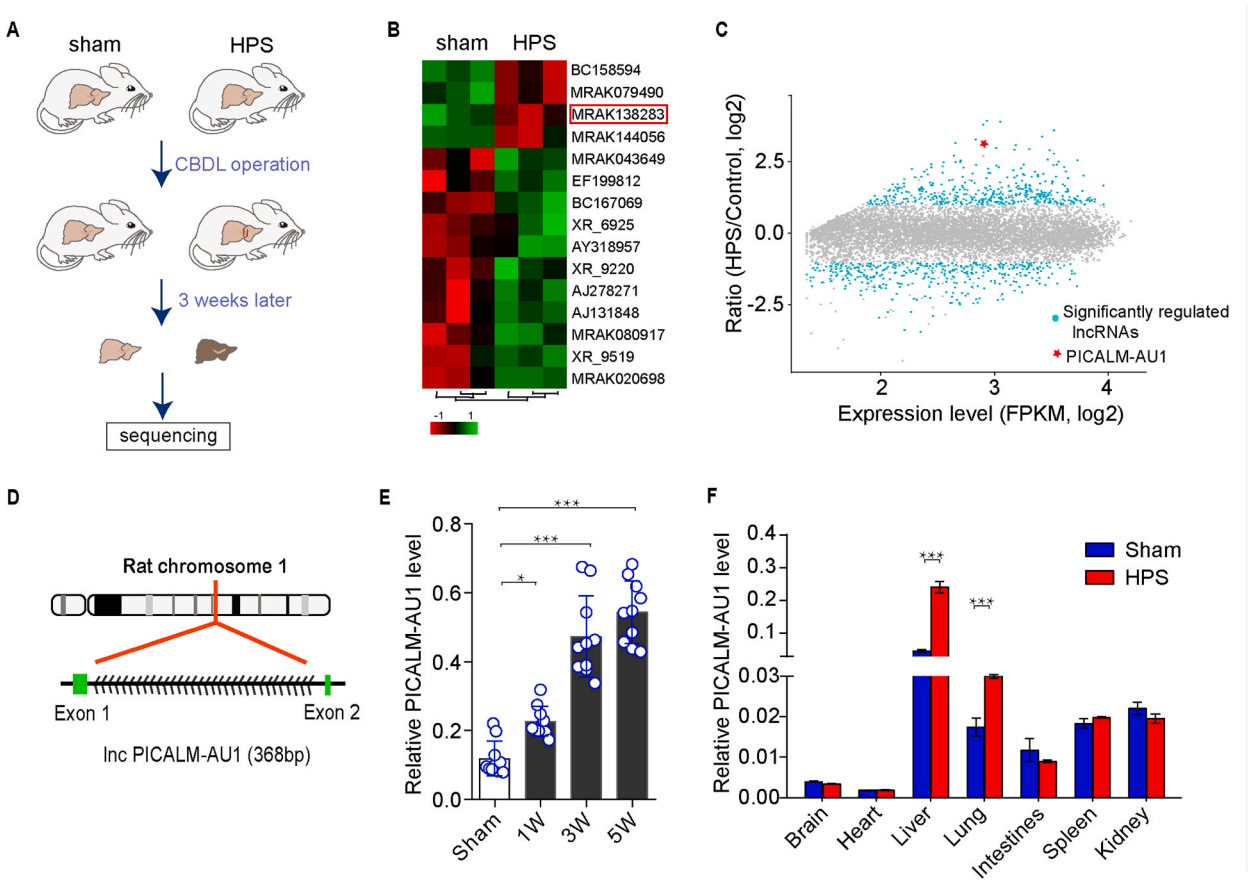

Fig. 1. lncRNA PICALM-AU1 was highly expressed in the HPS liver
(A) Strategy of Common bile duct ligation rat model construction. (B) Gene expression changes were assayed by deep sequencing of RNA Array. (C) Significantly regulated lncRNAs are highlighted in light blue, PICALM-AU1 is highlighted in red. (D) The structure and location of PICALM-AU1 in rat genomic chromosome. (E–F) qPCR analysis of PICALM-AU1 expression in the different stage of HPS rat liver and in different tissues at the third week of HPS rats.
Statistical significance relative to sham group, *P < 0.05, **P < 0.01, ***P < 0.001, n = 10, *t*-test.

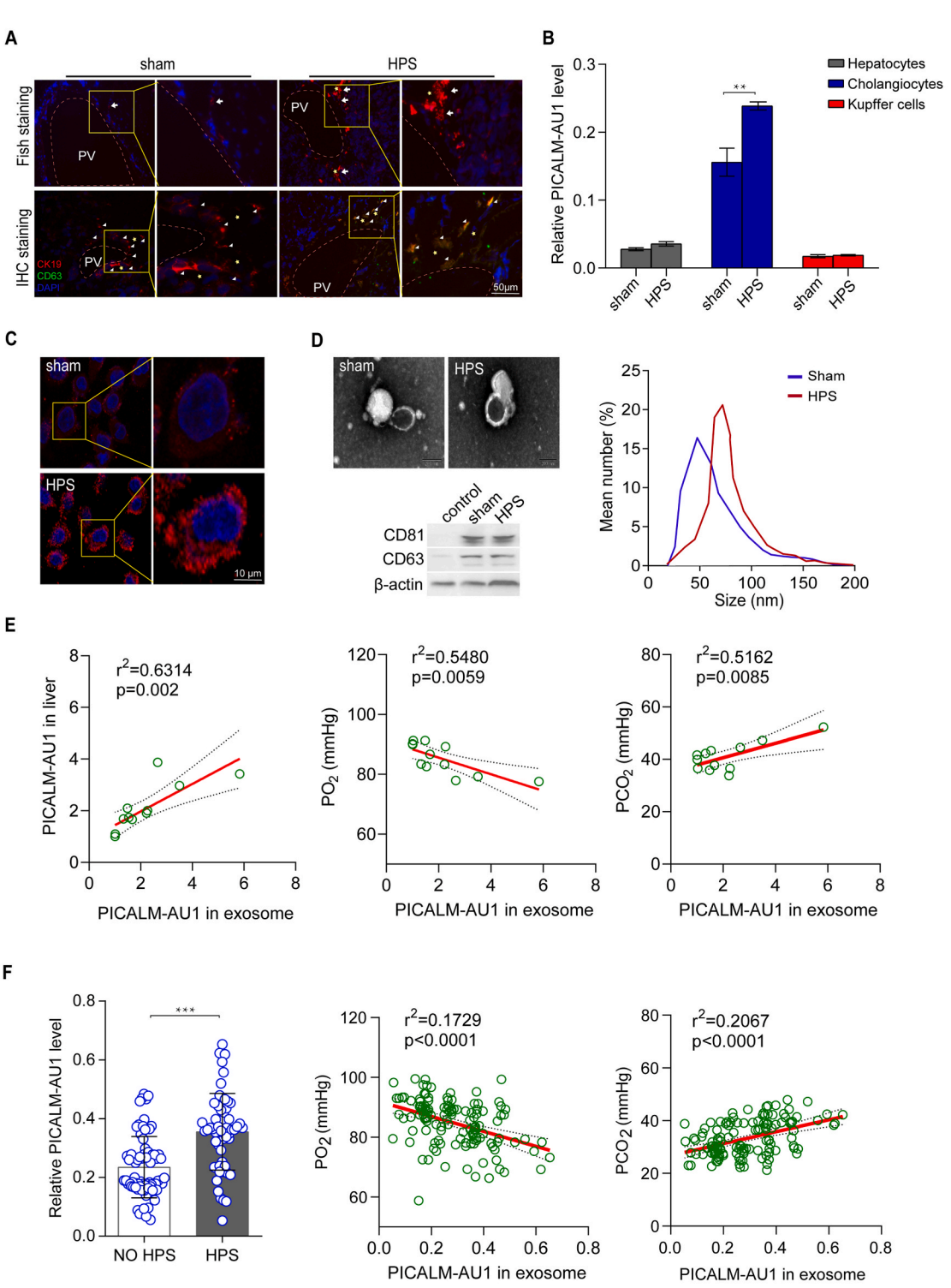

Fig. 2. PICALM-AU1 expressed in the cholangiocyte and released as exosome

(A) Representative images of FISH targeting PICALM-AU1 in liver are shown in upper line. Representative images of immunofluorescence targeting CK19 and CD63 are shown in lower line. Colocalization of CK19 and CD63 are indicated by white triangles. bile duct, yellow *; Portal vein, PV. **(B)** qPCR analysis PICALM-AU1 expression in the cholangiocytes, primary hepatocytes and Kupffer cells. **(C)** Subcellular localization of PICALM-AU1 in cholangiocyte cell by FISH staining.

(D) sham and HPS rat serum exosome were isolated and detected by the TEM (upper line) and Western blot (lower line), and the number of

exosomes were analyzed (right). **(E)** Correlation between hepatic PICALM-AU1 and serum exosomal PICALM-AU1 (left), PO_2 and exosomal PICALM-AU1 (middle), PCO_2 and exosomal PICALM-AU1 (right) was analyzed. **(F)** exosomal PICALM-AU1 expression was analyzed in 56 HPS patients and 73 chronic liver patients without HPS (left). The correlation between PO_2 and exosomal PICALM-AU1 (middle), PCO_2 and exosomal PICALM-AU1 was analyzed (right).

of intrapulmonary shunting could not be assessed using contrast-enhanced echocardiography.

2.8. Exosome isolation and characterization

Exosomes were isolated from human patient serum, rat serum, and MIBECs medium by differential centrifugation/ultracentrifugation protocols [31]. Briefly, samples were collected by centrifugation at 2000×*g* for 15 min, followed by 16,000×*g* for 20 min at 4 °C. Then, the supernatants were collected and ultracentrifuged at 110,000×*g* for 70 min. The pellets were resuspended in sterile PBS and purified by centrifugation at 110,000×*g* for 1 h. Subsequently, the exosomes were resuspended in PBS, filtered through a 0.22 μm filter (Millipore, USA), and then stored at −80 °C for further analysis.

Transmission electron microscopy (Hitachi HT7700, Japan) was used to characterize the morphology of the isolated exosomes. The size distribution of the isolated exosomes, was determined using qNano (Izon Science, New Zealand) following the manufacturer's instructions. To analyze the protein markers of the exosomes, western blotting was performed using anti-CD63 and anti-CD86 antibodies were used.

2.9. Statistical analysis

Results were obtained from at least three independent experiments and are expressed as mean ± SD. Data were analyzed by two-tailed student *t*-test, one way-variance analysis with Tukey's post-hoc test or linear regression using GraphPad Prism software version 8.0 (GraphPad Software Inc., USA). A *P* value of ≤0.05 was considered statistically significant.

3. Results

3.1. LncRNA PICALM-AU1 is highly expressed in the HPS liver

To identify the key lncRNAs regulate HPS progression, we constructed an HPS rat model by CBDL (Fig. 1A). The CBDL rats exhibited cirrhosis, low pulmonary gas exchange efficiency, and excessive pulmonary micro-vessels angiogenesis. RNA sequencing was performed to compare the liver RNA expression between CBDL and sham rats. After filtering the data for lnc RNA annotation, the expression levels of 88 lncRNAs were upregulated, and 10 lncRNAs were downregulated after CBDL (Fig.1BCE). The top 4 upregulated lncRNAs were selected as primary targets. Quantitative polymerase chain reaction (qPCR) showed that the lncRNA MRAK138283 was mostly upregulated in the early pathological phase of the CBDL rat liver (Fig. 1E). Therefore, we selected MRAK138283 (NCBI: LOC102550036) for further analysis. This novel lncRNA that has not been previously reported, and it is located on the antisense strand of rat chromosome 1 and upstream of Picalm. Thus, we named this lncRNA as "PICALM-AU1" and it had two exons of 368bp in the complete coding sequence (CDS) (Fig. 1D).

Furthermore, we analyzed PICALM-AU1 expression at the different time points in sham and CBDL rat livers. The results showed that the PICALM-AU1 level was the highest in the liver (Fig. 1F). The HPS rat liver was highly expressed in the first week, and its expression increased with time (Fig. 1E).

3.2. PICALM-AU1 is synthesized in cholangiocytes and secreted into the serum as exosomes

To determine the expression pattern of PICALM-AU1, we first examined its expression in the livers of sham and HPS rats using FISH staining. The expression of PICALM-AU1 was higher in HPS rat livers than that in the sham and CK19-positive cholangiocytes of 3-week-old CBDL rats (Fig. 2A). We then separated the three main cell types in the liver (cholangiocyte cells, Kupffer cells and Hepatocyte cells) to detect whether PICALM-AU1 was synthesized in the cholangiocyte. The qPCR showed that PICALM-AU1 mRNA was highly and predominantly expressed in cholangiocytes compared with its expression in the other two cell types. The PICALM-AU1 levels in the HPS group were 30 % higher than those in the sham group (Fig. 2B). FISH staining of the cholangiocytes showed that PICALM-AU1 was mainly localized in the cytoplasm and nucleus (Fig. 2C).

Given that PICALM-AU1 is expressed mainly in liver cholangiocytes and located in the cytoplasm, we proposed that that PICALM-AU1 may be secreted from liver cholangiocytes as exosomes and function in the lungs. Therefore, we isolated exsomes from sham and HPS rats and measured the expression of PICALM-AU1 (Fig. 2D). The correlation analysis showed that hepatic PICALM-AU1 mRNA levels were positively correlated with those of the serum exosomes (Fig. 2E, left panel). Furthermore, IHC staining for CD63, an exosome surface marker, indicated that CD63 was expressed and up-regulated in the cholangiocytes (Fig. 2A, lower line). These results indicated that PICALM-AU1 is expressed in cholangiocytes and secreted into the serum as an exosome.

Levels of serum exosomal PICALM-AU1 are correlated with the severity of HPS in the rat model and in human patients.

To identify the function of exosomal PICALM-AU1 in the pathological angiogenesis of HPS, the relationship between PICALM-AU1 and gas exchange in HPS rats was investigated. The correlation analysis showed PICALM-AU1 in exosomes was positively correlated

with carbon dioxide (PCO_2), and negatively with the partial pressure of partial pressure of oxygen (PO_2) (Fig. 2E, middle and right panels).

To confirm these results, 56 HPS patients with chronic cirrhosis and 73 control chronic cirrhosis patients without HPS were included in this study. Based on the basic information, patients with HPS had vertical dyspnea and were positive for Type-B ultrasound. Patients with HPS had a higher partial pressure of carbon dioxide in artery, and a lower partial pressure of oxygen in the artery than those without HPS (Table 1). Serum exo-PICALM-AU1 levels were significantly higher in patient with HPS than that without HPS (Fig. 2F, left panel). Serum exosomal PICALM-AU1 levels were negatively correlated with PO_2; however, they were positively correlated with PCO_2 (Fig. 2F, middle and right panels). This indicates that serum exosomal PICALM-AU1 is associated with the pathological formation and development of HPS.

3.3. Exo-PICALM-AU1 promoted PMVECs EndMT in rat lung

The endothelial-mesenchymal transition plays an important role in regulating angiogenesis and blood vessel remodeling [32]. Immunohistochemistry and western blotting were used to confirm the function of EndMT in HPS lungs. Endothelial biomarker VE-cadherin and mesenchymal cell biomarker vimentin expression were detected during HPS progression. The results showed that VE-cadherin expression was reduced. In contrast, vimentin expression was induced in the rat lung during the HPS period (Figs. S1A and B). These data suggested that EndMT is occurs during pathological pulmonary micro-vascular angiogenesis.

To determine whether exosome-derived PICALM-AU1 stimulates EndMT in PMVECs in vivo, we used HPS-derived exosome treated normal rats. To confirm PICALM-AU1 function, normal rats were treated with exosomes from the MIBECs cell line, with MIBECs overexpressing PICALM-AU1. This strategy is illustrated in Fig. 3A. Quantitative PCR was used to detect the expression of EndMT-related genes. VE-cadherin mRNA transcription in HPS rat-derived exosomes was reduced by 35 % compared with that in the sham-serum exosomes. The VE-cadherin mRNA level in the PICALM-AU1 overexpression MIBECs-derived exosome treatment was reduced by 45 % compared with that in the control exosomes. *Vimentin*, TGFβ, and collagen 1 mRNA transcription were significantly induced after HPS rat exosome treatment or PICALM-AU1 overexpression (Fig. 3B). Moreover, immunohistochemical staining confirmed that VE-cadherin expression was reduced by the HPS rat-derived exosome treatment and the PICALM-AU1 overexpression MIBECs-derived exosome treatment. However, vimentin expression showed the opposite trend (Fig. 3C).

To investigate whether EndMT in lung PMVECs was induced by PICALM-AU1, CBDL rats were treated with PICALM-AU1 overexpression or PICALM-AU1 knockdown using an adeno-associated virus. The experimental setup is illustrated in Fig. 3D. The pathological changes in rats were more serious, and VE-cadherin mRNA transcription and protein expression were reduced in the PICALM-AU1 overexpression virus control rats compared with those in the HPS group or sham group. In contrast, vimentin expression was the opposite of VE-cadherin expression. The PICALM-AU1 knockdown virus treatment partially reversed HPS pathology and relevant gene synthesis (Fig. 3E and F).

To confirm that exo-PICALM-AU1 can promote EndMT in PMVECs in vitro, we first used exosomes from HPS rat serum and exosomes from MIBECs (which have overexpressed PICALM-AU1 in the MIBEC line by lentivirus) to treat PMVECs. The PMVEC proliferation and migration were induced by HPS- and MIBECs-derived exosomes, which overexpressed PICALM-AU1 (Fig. 4A,B,C). An adeno-associated virus overexpressing PICALM-AU1 induced PMVEC proliferation and migration. However, the adeno-associated virus with PICALM-AU1 knockdown inhibited PMVEC proliferation and migration (Fig. 4D,E,F). These results suggest that serum exosomal PICALM-AU1 induces EndMT in HPS rat lung PMVECs and promotes HPS pathological progression in rats.

Table 1
Basic feature of HPS patients.

Prognostic variables	NO HPS (N = 73)	HPS (N = 56)	χ2	P value
Age at diagnosis, median (min, max), y	44 (18, 75)	51.5 (21, 75)		
Sex, male (female) [ratio]	55 (18) [75.3 %]	44 (12.0) [78.6 %]		
median (min, max), cm	168 (148, 177)	165 (150, 180)		
median (min, max), kg	61 (39, 90)	64.5 (42, 96)		
pathology, (hepatitis B/others)	45/28	43/13	3.351	0.086
Aspartate transaminase, AST, U/L	94.09 ± 89.1	114.31 ± 84.74		0.913
Cerealthirdtransaminase, ALT, U/L	144.35 ± 190.59	88.91 ± 78.2		0.001
Albumin, mg/dl	35.06 ± 4.91	30.74 ± 4.8		0.867
Globulin, GLB, mg/dl	30.43 ± 7.3	31.53 ± 7.84		0.237
prothrombin time, PT	13.98 ± 3.5	18.77 ± 5.07		0.003
Meld index	61.94 ± 6.38	67.56 ± 7.11		0.22
Vertical dyspnea, (Yes/No)	18/55	40/16	28.014	<0.0001
partial pressure of oxygen in artery	98.56 ± 2.65	86.92 ± 19.11		0.027
partial pressure of carbon dioxide in artery	38.86 ± 2.67	35.97 ± 4.12		0.001
alveolar-arterial oxygen tension difference, P(A-a)O2, mmHg	8.62 ± 6.91	28.56 ± 8.52		0.023
Type-B ultrasonic, (positive/negative)	16/57	56/0	70.891	<0.0001
Clubbing digits	27/46	23/33	5.13	0.024
Spider angioma	7.03 ± 4.68	5.2 ± 3.82	25.745	0.041

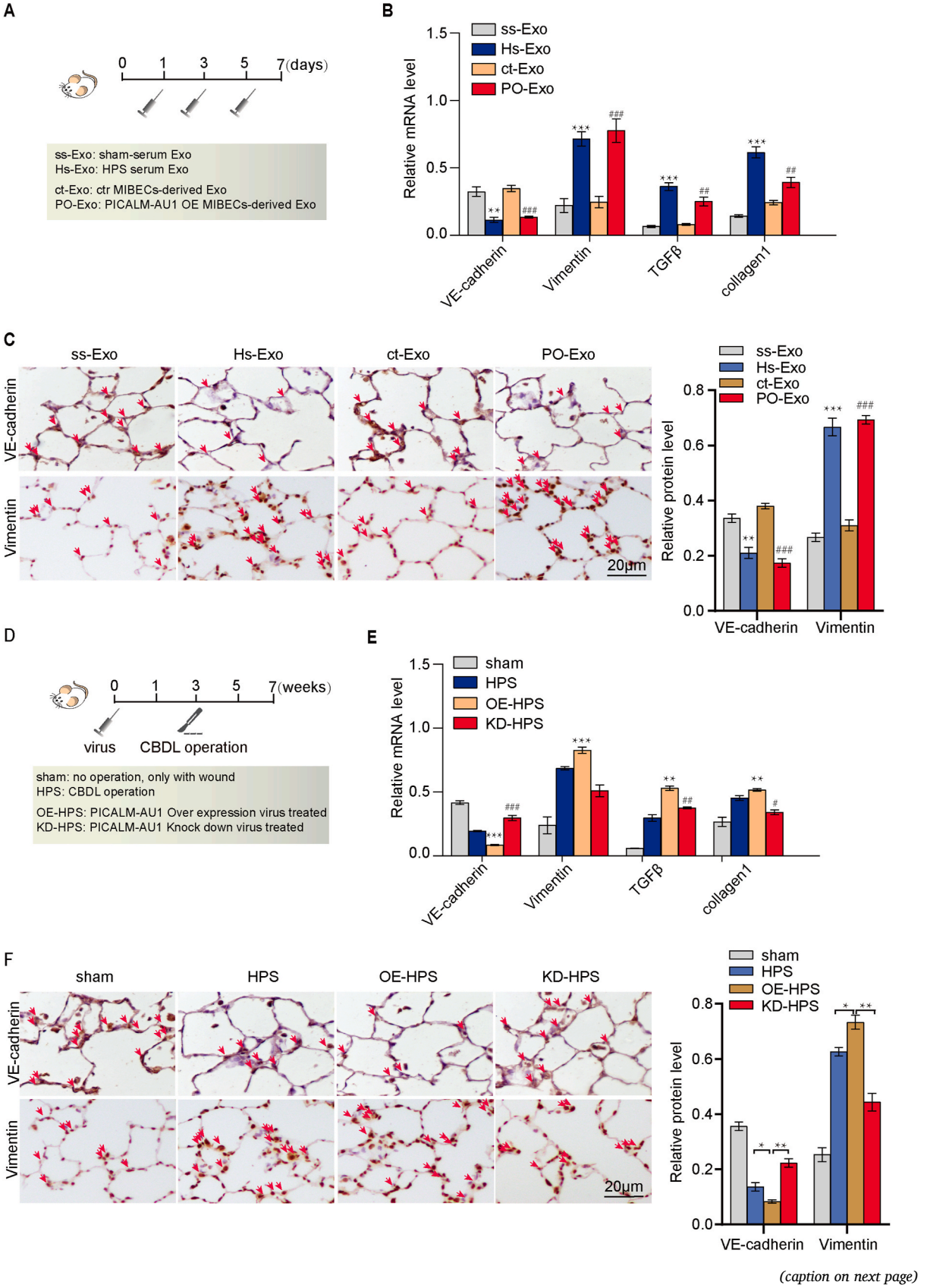

(caption on next page)

Fig. 3. Exo-PICALM-AU1 promoted PMVECs EndMT
(A) Experimental protocol of exosomes treated rat. (B) Relative mRNA level was detected by qPCR. Statistical significance relative to ss-Exo treated group, *P < 0.05, **P < 0.01, ***P < 0.001; relative to ct-Exo treated group, #P < 0.05, ##P < 0.01, ###P < 0.001, n = 5. (C) IHC showed endothelia cell marker (VE-cadherin) expressed reduce and mesenchymal cell marker (Vimentin) expressed induced during the HPS rat lung; (ss-Exo, Serum exosomes from sham rat; HPS-Exo, serum exosomes from 3-week CBDL rat; ct-Exo, exosomes from the culture medium of control MIBECs cells; PO-Exo, exosomes from PICALM-AU1 over expression MIBECs cells). (left, IHC staining; Right, Quantification of related proteins). (D) Experimental protocol of PICALM-AU1 over expression and knockdown in HPS rat. (E) Relative mRNA level was detected by qPCR. Statistical significance relative to sham group, *P < 0.05, **P < 0.01, ***P < 0.001; relative to HPS group, #P < 0.05, ##P < 0.01, ###P < 0.001, n = 5. Data were compared by 2-way ANOVA. (F) IHC showed endothelia cell marker (VE-cadherin) expressed reduce and mesenchymal cell marker (Vimentin) expressed induced during the HPS rat lung. (left, IHC staining; Right, Quantification of related proteins).

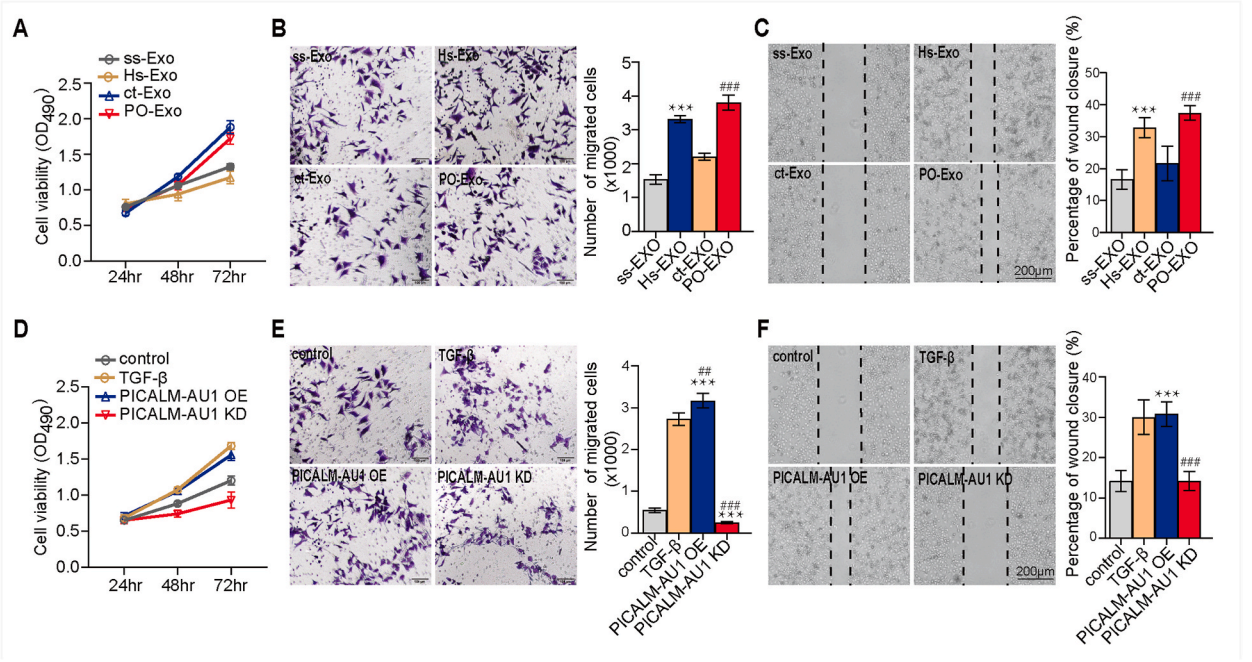

Fig. 4. Exo-PICALM-AU1 promoted PMVECs proliferation and migration
(A-C) Exosomes treated PMVECs cell. HPS rat serum derived exosome and Over expression MIBECs cells derived exosome induce PMVECs proliferation (A) and migration (B, C), statistical significance relative to ss-Exo treated group, *P < 0.05, **P < 0.01, ***P < 0.001; relative to ct-Exo treated group, #P < 0.05, ##P < 0.01, ###P < 0.001, n = 5.
(D–F) PICALM-AU1 over expression and knockdown lentivirus treated PMVECs cell. D, over expression of PICALM-AU1 induce PMVECs proliferation (D) and migration (E, F), PICALM-AU1 knock down reduce PMVECs proliferation and migration. Statistical significance relative to control, *P < 0.05, **P < 0.01, ***P < 0.001; relative to TGFβ, #P < 0.05, ##P < 0.01, ###P < 0.001, n = 5. Data were compared by 2-way ANOVA.

*3.4. MicroRNA 144-3p is a **PICALM-AU1 target***

To investigate how PICALM-AU1 regulates EndMT in PMVECs, we first analyzed the gene expression network in the HPS lungs by microarray (unpublished data). We observed that miR144-3p is a putative target of PICALM-AU1 (Fig. S2). An miR144-3p binding site was observed in the PICALM-AU1 sequence (Fig. 6C). We previously observed that miR144-3p could inhibit PMVEC proliferation in HPS lungs [4]. This indicates that PICALM-AU1 may regulate EndMT by miR144-3p.

To confirm the relationship between PICALM-AU1 and miR144-3p, the HPS rat model, exosome-treated rat model, and recombinant adeno-associated virus-mediated PICALM-AU1 overexpression/knockdown were used to treat HPS rats. In the rat model, miR144-3p expression rapidly decreased with HPS development. This trend was opposite that of PICALM-AU1 (Fig. 5A). In an exosome-treated rat model, miR144-3p expression was reduced by HPS rat serum exosomes. The miR144-3p expression level was opposite to that of PICALM-AU1 (Fig. 5B). This result was confirmed in a rat model treated with a recombinant adeno-associated virus. When PICALM-AU1 was overexpressed, miR144-3p mRNA levels were reduced. In the PICALM-AU1 knockdown, miR144-3p mRNA levels increased (Fig. 5C). The results showed that miR144-3p is a potential target of PICALM-AU1, and its expression was negatively correlated with that of PICALM-AU1 in the lungs of HPS rats.

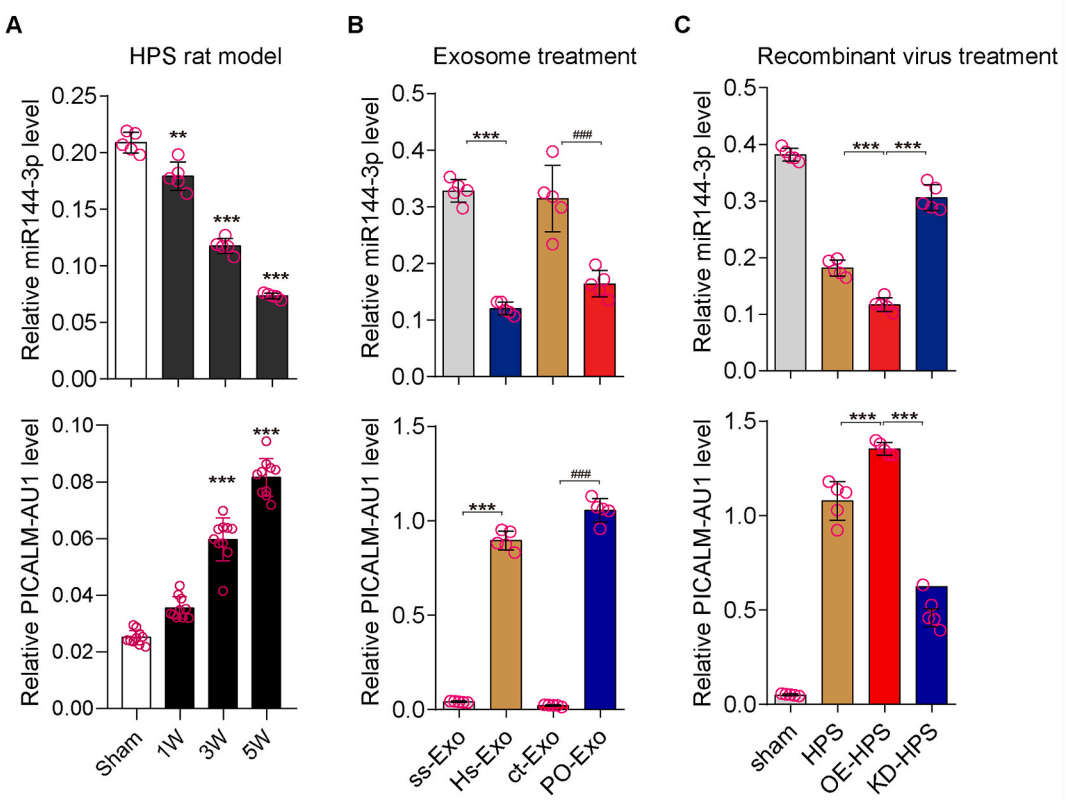

Fig. 5. miR144-3p is reduced by PICALM-AU1
(A) The expression trend of miR144-3p and PICALM-AU1 in HPS rat lung; (B) miR144-3p, PICALM-AU1 mRNA level in exosome treatment rat model; (C) miR144-3p, PICALM-AU1 mRNA level in exosome treatment rat model. *P < 0.05, **P < 0.01, ***P < 0.001; #P < 0.05, ##P < 0.01, ###P < 0.001, n = 5. Data were compared by 2-way ANOVA.

3.5. *PICALM-AU1 inhibited miR144-3p*

First, to identify whether miR144-3p regulates EndMT in PMVECs, we used miR144-3p mimics and inhibitors. The immunofluorescence analysis showed that miR144-3p overexpression promoted EndMT by inducing vimentin expression and reducing VE-cadherin expression. The reduction in miR144-3p inhibited EndMT by suppressing vimentin expression (Fig. 6A and B).

To analyze the regulatory function of PICALM-AU1 on miR144-3p, we constructed a luciferase reporter system (Fig. 6C). The psiCHECK2 vector with Tie2 3′UTR (with miR144-3p binding sites, as reported in our previous work [4]) downstream of the LUC gene was transfected into the PMVECs line. Next, the miR144-3p mimic and inhibitor were used to treat PMVECs to upregulate and downregulate the miR144-3p levels, respectively. Nuclear fragments of PICALM-AU WT and PICALM-AU1 MUT were used to overexpress PICALM-AU1. When the mutated PICALM-AU1 nuclear fragment was transfected into the PMVECs, the miR144-3p mimic reduced LUC activity by 20 %, while the miR144-3p inhibitor induced LUC activity by 1.5-fold. When the wild-type PICALM-AU1 nuclear fragment was transfected into the PMVECs, the reduction in LUC activity caused by the miR144-3p mimic was recovered. The LUC activity reached a maximum in the miR144-3p inhibitor-treated PMVECs (Fig. 6D). This indicated that PICALM-AU1 negatively regulated miR144-3p levels in the PMVECs.

To confirm this result, we used PICALM-AU1 overexpression and knockdown of lentivirus-treated PMVECs. Luciferase assays showed that PICALM-AU1 overexpression increased Luc activity by 1.6-fold. However, the PICALM-AU1 knockdown reduced Luc activity by 25 % (Fig. 6E). These results suggest that PICALM-AU1 regulates EndMT by inhibiting miR144-3p levels.

3.6. *MicroRNA **144-3p inhibited PMVEC EndMT by** the **ZEB1 transcriptional factor***

To analyze the role of miR144-3p in regulating EndMT, target genes were predicted using the miRWalk and miRtarBase websites (http://mirwalk.umm.uni-heidelberg.de/and http://mirtarbase.mbc.nctu.edu.tw/php/index.php, respectively). We observed that ZEB1 is a miR144-3p putative target gene (Table S3). Additionally, known as Zinc Finger E-Box Binding Homeobox 1, ZEB1 acts as a transcriptional repressor and inhibits interleukin-2 gene expression [33], and it represses the E-cadherin promoter and induces epithelial-mesenchymal transition by recruiting SMARCA4/BRG1 [17,33,34]. Therefore, we first overexpressed or knocked down miR144-3p using specific mimics and inhibitors and detected ZEB1, SNAIL, TWIST, and SLUG gene transcripts by qPCR. The results

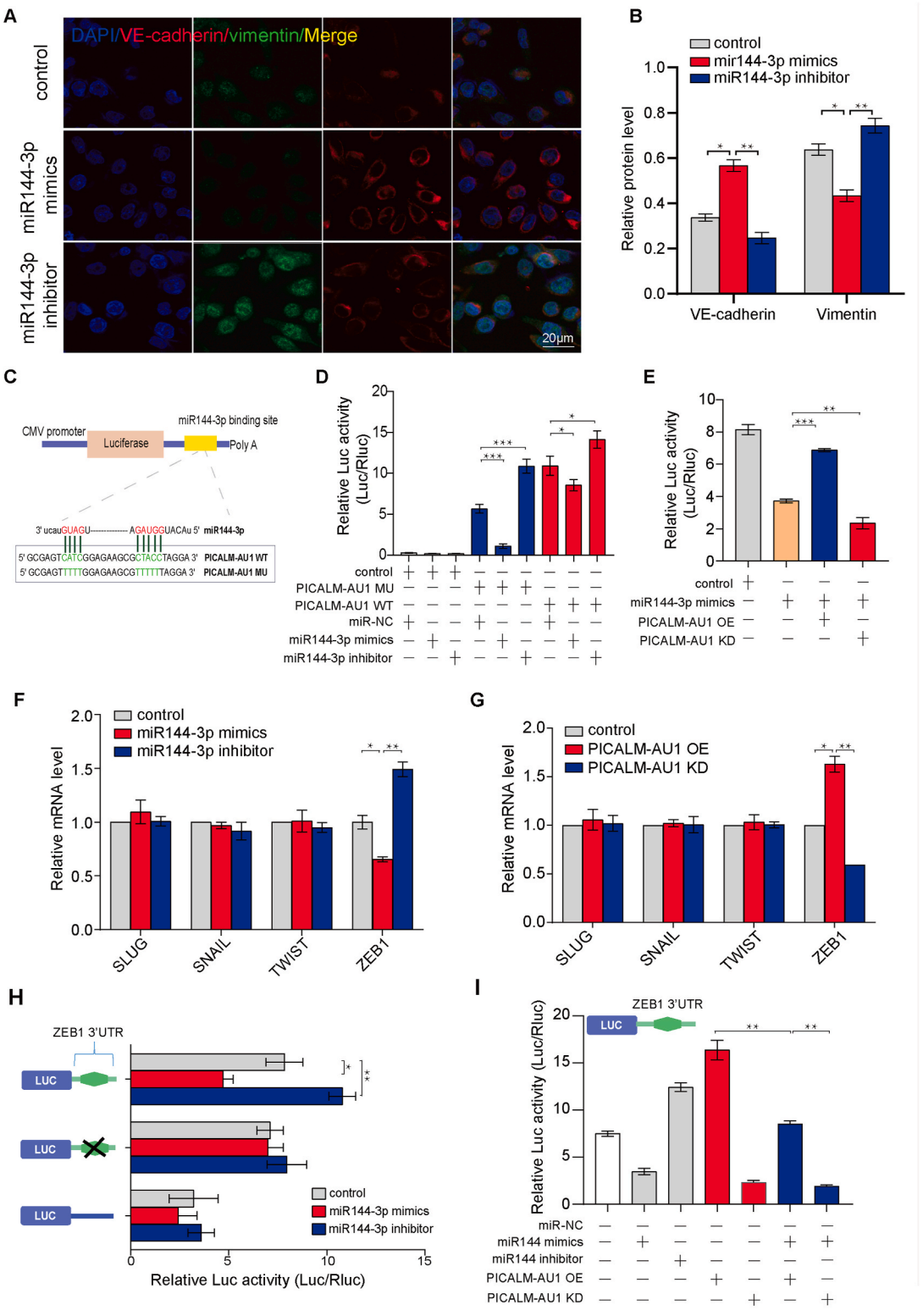

Fig. 6. PICALM-AU1 promotes PMVECs EndMT by inhibiting miR144-3p/Zeb1
(A) IF analysis VE-cadherin and vimentin stain in the miR144-3p mimics and inhibitor treatment PMVECs. **(B)** Quantification of related proteins expression in PMVECs. **(C)** Schematic outline of predicted binding sites for miR144-3p on Lnc PICALM-AU1. **(D)** Luciferase activity of psiCHECK2-PICALM-AU1 and psiCHECK2-PICALM-AU1mut upon transfection of indicated miRNA mimics in PMVECs (n = 3). psiCHECK2-miR144-3p (3 ×)

was used as positive control. Data are presented as the ratio of Renilla luciferase activity to Firefly luciferase activity. **(E)** Luciferase activity of psiCHECK2-PICALM-AU1 upon PICALM-AU1 overexpression or knock down lentive virus treated PMVECs. **(F)** qPCR analysis key EndMT relative transcriptional factors expression after miR144-3p up-regulated and down-regulated in PMVECs. (G) qPCR analysis key EndMT relative transcriptional factors expression by PCALM-AU1 up-regulated and down-regulated in PMVECs. (H) Dure luciferances assay analysis miR144-3p inhibit ZEB1 expression. (I) Dure luciferances assay analysis PICALM-AU1 regulated miR144-3p/ZEB1 expression.

showed that the ZEB1 transcript in the PMVECs was reduced by the miR144-3p mimic treatment and induced by the miR144-3p inhibitor treatment (Fig. 6F). We then overexpressed or knocked down PICALM-AU1 in the PMVECs. The results showed that the ZEB1 transcript in the PMVECs was induced when PICALM-AU1 was overexpressed and reduced by the PICALM-AU1 knockdown (Fig. 6G). Next, we used a dual-luciferase assay to analyze the miR144-3p-mediated regulation of ZEB1. The vector with ZEB1 3′UTR was transfected into the PMVECs, and the cell line was treated with miR144-3p mimics and miR144-3p inhibitors. The results showed miR144-3p can bind with ZEB1 3′UTR and inhibit Luc activity. When the binding site was disrupted, miR144-3p no longer inhibited Luc activity (Fig. 6H). We further overexpressed PICALM-AU1 based on a dual-luciferase assay in the PMVECs, which partially recovered the Luc activity by miR144-3p inhibition (Fig. 6I). These results showed that miR144-3p can inhibit EndMT in PMVECs via ZEB1 and that PICALM-AU1 can promote EndMT by inhibiting miR144-3p.

3.7. PICALM-AU1 promoted PMVEC EndMT by miR144-3p/ZEB1

To identify whether PICALM-AU1 regulates PMVEC EndMT via miR144-3p/ZEB1, PMVECs were treated with sham and HPS rat serum exosomes. Immunofluorescence, qPCR, and western blotting showed that ZEB1 expression was induced, and VE-cadherin, N-cadherin, and ZO-1 expression were reduced after the HPS exosome treatment compared with that in the sham exosome treatment (Fig. 7A,B,C). The overexpression and knockdown of PICALM-AU1 were achieved using a recombinant adenovirus. Immunofluorescence, qPCR, and western blotting showed that ZEB1 expression was induced while VE-cadherin and ZO-1 expression were reduced after PICALM-AU1 overexpression. In contrast, ZEB1 expression was reduced while VE-cadherin and ZO-1 expression were induced after PICALM-AU1 knockdown compared with that in the control (Fig. 7D,E,F). These results showed that PICALM-AU1, synthesized from liver cholangiocytes, secreted into exosomes, and functioning in the HPS lung, promoted PMVEC EndMT via miR144-3p/ZEB1.

4. Discussion

We previously focused on the mechanism of pulmonary microvascular remodeling and how to block it to improve HPS pathology [35–40]. However, the effect is limited. Then we think, the pathological of HPS is come from liver disease. So, the secretion of liver is the key factor to make HPS development. In our recently study, we found a c-kit^{+} cell was collected into lung by serum SDF1 which may participate in angiogenesis of pulmonary microvascular [41]. In this study, we identified the lncRNA PICALM-AU1, which is expressed mainly in the cholangiocytes of the liver and is secreted as exosomes. We showed that cholangiocyte-derived lncRNA PICALM-AU1 plays a pivotal role in activating EndMT in PMVECs and promoting excessive angiogenesis in HPS.

The newly discovered lncRNA PICALM-AU1 has two exons of 368 bp in the complete CDS. Under normal physiological conditions, PICALM-AU1 expression is low in all tissues. However, PICALM-AU1 levels were dramatically increased in the liver and lungs of HPS rats. In this study, we identified cholangiocytes as the primary source of hepatic PICALM-AU1 under physiological and cholestatic conditions using three approaches: immunopurification of primary cholangiocytes, laser capture microdissection, and FISH-IHC.

Exosomal PICALM-AU1 plays a critical role in the pathological angiogenesis of HPS in rat lungs. Exosomes are small extracellular vesicles released by various cell types that can carry multiple cargoes, including proteins, DNA, mRNA, lncRNA, and lipids [42–45]. Recently, exosomes have attracted considerable attention as essential mediators of intercellular communication under both physiological and pathological conditions [42]. The endothelial-mesenchymal transition is thought to be a core factor contributing to the accumulation of pulmonary microvascular formation and recapitulating the pathways associated with HPS development. EndMT may be reversible [31]. Thus, insights into the mechanisms controlling EndMT are relevant to vascular remodeling and important for developing new therapies aimed at reversing vascular remodeling to relieve pain in patients with HPS. This study focuses on the characteristics, functions, and roles of EndMT in HPS vascular remodeling.

5. Conclusion

In summary, we explored the role of PICALM-AU1 in regulating EndMT in HPS pathological blood vessel remodeling via exosome-mediated communication between distant organs. This study provides a future clinical perspective on exo-PICALM-AU1 signaling for therapeutics after severe liver injury. The limitation of this study is that the interaction between PICALM-AU1 and miR144-3p need more directly experimental evidence. We believe that the design of PICALM knockout mice will have more important significance for the study of the biological function of this molecule and will lead to more discoveries. In fact, the potential clinical implications of the findings, we have developed a clinical detection kit based on this molecule for the early diagnosis of HPS, and have applied patent. Furthermore, we will use the kit on further clinical demonstration. Secondly, PICALM-AU1 is also a potential point to HPS targeted therapy.

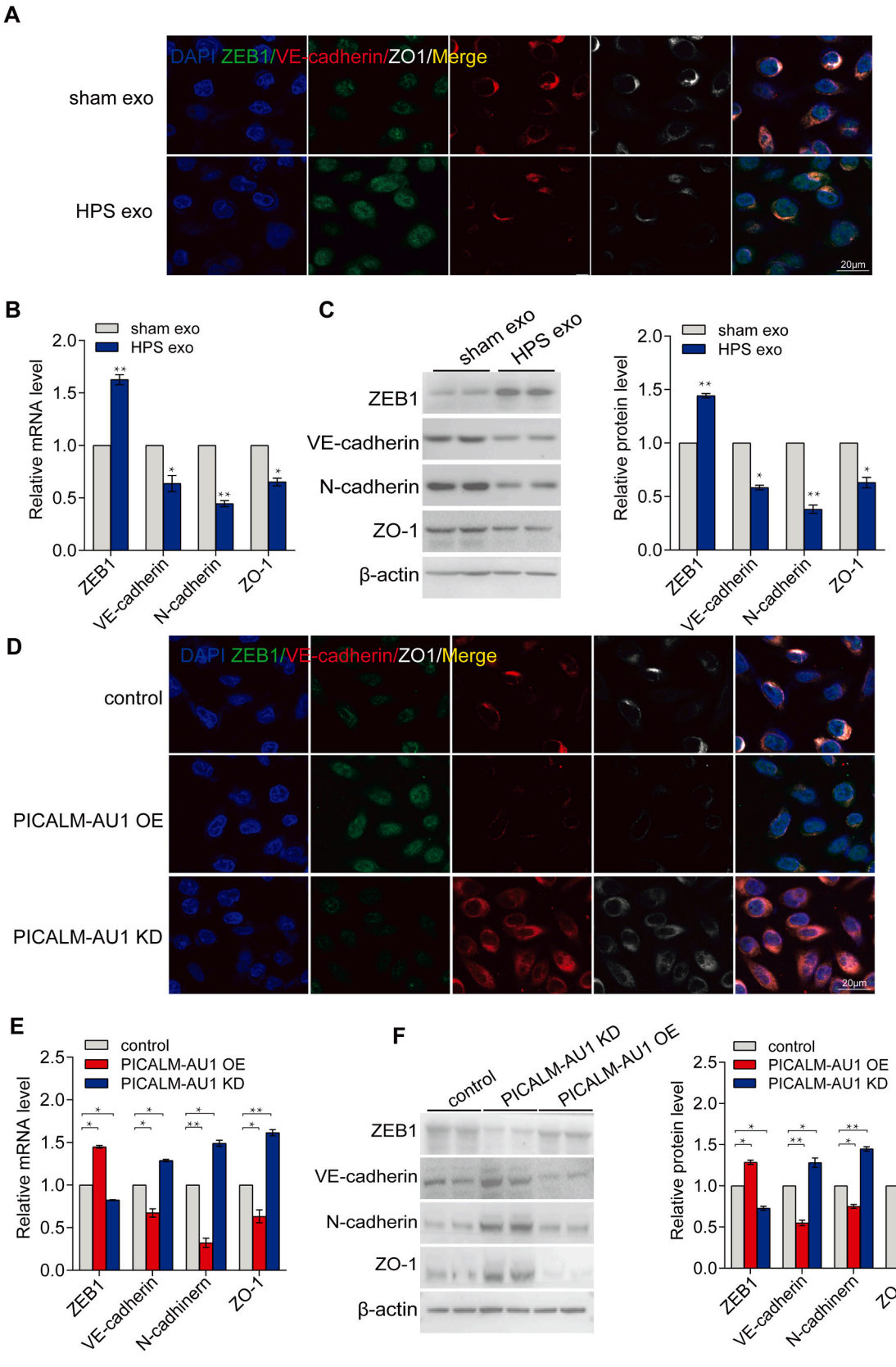

(caption on next page)

Fig. 7. PICALM-AU1 induced PMVECs EndMT by inhibiting miR144-3p/ZEB1
(A–C) IF, qPCR and Western blot showed ZEB1 expression was induced and VE-cadherin and ZO-1 expression was reduced after HPS exosome treatment than that of sham exosome treatment;
(D–F) IF, qPCR and Western blot showed ZEB1 expression was induced and VE-cadherin, ZO-1 expression was reduced after PICALM-AU1 over expression than that of control. And ZEB1 expression was reduced and VE-cadherin, ZO-1 expression was induced after PICALM-AU1 knockdown than that of control.

Clinical perspectives

1.The potential role of a novel lncRNA, PICALM-AU1 in EndMT of HPS and its underlying mechanisms were explored.
2.Aberrant up-regulation of PICALM-AU1 induces ZEB1 expression and regulates EndMT progression by sponging with miR144-3p.
3.Our findings establish a critical role for PICALM-AU1 regulates pathological angiogenesis in HPS and provide a new determinant pathological factor and potential target for the prevention of HPS.

Data availability statement

The data that support the findings of the present study are available from the corresponding author upon reasonable request.

Funding

This project was supported by the National Natural Science Foundation of China (81800060, 81671961, 81700046) and Natural Science Foundation of Chongqing, China (cstc2020jcyj-msxmX0361) and The Science and Technology Project Affiliated to the Education Department of Chongqing Municipality (KJZD-K202215104).

CRediT authorship contribution statement

Congwen Yang: Writing – original draft, Resources, Methodology, Investigation, Funding acquisition, Data curation. **Yihui Yang:** Software, Resources, Methodology, Data curation. **Yang Chen:** Software, Methodology. **Jian Huang:** Methodology. **Dan Li:** Writing – review & editing, Validation, Software. **Xi Tang:** Methodology. **Jiaolin Ning:** Methodology. **Jianteng Gu:** Software. **Bin Yi:** Writing – review & editing, Resources. **Kaizhi Lu:** Writing – review & editing, Writing – original draft, Visualization, Supervision, Conceptualization.

Declaration of competing interest

The authors declare that they have no known competing financial interests or personal relationships that could have appeared to influence the work reported in this paper.

Abbreviations

HPS	Hepatopulmonary Syndrome
EndMT	Endothelial stromal transformation
PMVECs	pulmonary microvascular endothelial cells
MIBECs	mice intrahepatic biliary epithelial cells
ZEB1	Zinc Finger E-Box Binding Homeobox 1
OE	Over expression; KD, knowck down
ss-Exo	serum of sham rat derived exosome
Hs-Exo	serum of HPS rat derived exosome
ct-Exo	control of MIBECs derived exosome
PO-Exo	PICALM-AU1 Over expression MIBECs-derived exosome

Appendix A. Supplementary data

Supplementary data to this article can be found online at https://doi.org/10.1016/j.heliyon.2024.e24962.

References

[1] Rodríguez-Roisin, et al., Hepatopulmonary Syndrome — A Liver-Induced Lung Vascular Disorder, The New England, J. Med. 358 (2008) 2378–2387.
[2] M.B. Fallon, et al., Impact of Hepatopulmonary Syndrome on Quality of Life and Survival in Liver Transplant Candidates, Gastroenterology, 135 (4) (2008) 1168–1175.

[3] C. Lejealle, et al., Evidence for an Association between Intrahepatic Vascular Changes and the Development of Hepatopulmonary Syndrome, Chest 155 (2018) 123–136.
[4] C. Yang, et al., miR144-3p Inhibits PMVECs Excessive Proliferation in Angiogenesis of Hepatopulmonary Syndrome via Tie2, Exp. Cell Res. 365 (2018) 24–32.
[5] C.C. Shen, et al., AMD3100 treatment attenuates pulmonary angiogenesis by reducing the c-kit (+) cells and its pro-angiogenic activity in CBDL rat lungs, Biochim. Biophys. Acta, Mol. Basis Dis. 1864 (3) (2018) 676–684.
[6] J. Zhang, et al., Pulmonary angiogenesis in a rat model of hepatopulmonary syndrome,, Gastroenterology 136 (3) (2009) 1070–1080.
[7] S. Raevens, et al., Placental growth factor inhibition targets pulmonary angiogenesis and represents a novel therapy for hepatopulmonary syndrome in mice, Hepatology 68 (2) (2017) 634–651.
[8] C. Liu, et al., Cyclooxygenase-2 Promotes Pulmonary Intravascular Macrophage Accumulation by Exacerbating BMP Signaling in Rat Experimental Hepatopulmonary Syndrome, Biochem Pharmacol 138 (2017) 205–215.
[9] C. Liu, et al., Bone morphogenic protein-2 regulates the myogenic differentiation of PMVECs in CBDL rat serum-induced pulmonary microvascular remodeling, Exp. Cell Res. 336 (1) (2015) 109–118.
[10] C. Fischer, et al., Anti-PlGF inhibits growth of VEGF(R)-inhibitor-resistant tumors without affecting healthy vessels, Cell 131 (3) (2007) 463–475.
[11] M. Shirley, et al., The Therapeutic Potential of Targeting the Endothelial-To-Mesenchymal Transition, Angiogenesis 22 (2018) 3–13.
[12] Li, et al., Reassessing Endothelial-To-Mesenchymal Transition in Cardiovascular Diseases, Nat Rev Cardiol 15 (8) (2018) 445–456.
[13] X Lin, A.C. Dudley, et al., Fine-Tuning Vascular Fate during Endothelial–Mesenchymal Transition, J Pathol 241 (1) (2017) 25–35.
[14] M. Wesseling, et al., The Morphological and Molecular Mechanisms of Epithelial/endothelial-To-Mesenchymal Transition and its Involvement in Atherosclerosis, Vascul Pharmacol 106 (2018) 1–8.
[15] K.M. Takada, et al., Contribution of Endothelial-to-Mesenchymal Transition to the Pathogenesis of Human Cerebral and Orbital Cavernous Malformations, Neurosurgery 81 (1) (2017) 176–183.
[16] N. Coll-Bonfill, et al., Transdifferentiation of endothelial cells to smooth muscle cells play an important role in vascular remodelling, Am J Stem Cells 4 (1) (2015) 13–21.
[17] B.C. Cooley, et al., TGF- Signaling Mediates Endothelial-to-Mesenchymal Transition (EndMT) During Vein Graft Remodeling, Sci Transl Med 6 (227) (2014) 227–234.
[18] N. Clere, S. Renault, I. Corre, Endothelial-to-Mesenchymal transition in cancer, Front. Cell Dev. Biol. 8 (2020) 747–755.
[19] S.S. Sohal, Endothelial to mesenchymal transition (EndMT): an active process in Chronic Obstructive Pulmonary Disease (COPD)? Respir Res 17 (20) (2016) 1–4.
[20] S. Reimann, et al., Increased S100A4 Expression in the Vasculature of Human COPD Lungs and Murine Model of Smoke-Induced Emphysema, Respir Res 16 (2015) 127–139.
[21] K.S. Visan, R.J. Lobb, A. Moller, The role of exosomes in the promotion of epithelial-to-mesenchymal transition and metastasis, Front. Biosci. 25 (6) (2020) 1022–1057.
[22] Z. Zeng, et al., Cancer-derived exosomal miR-25-3p promotes pre-metastatic niche formation by inducing vascular permeability and angiogenesis, Nat Commun 9 (1) (2018) 5395–5408.
[23] X. Loyer, et al., Intra-cardiac release of extracellular vesicles shapes inflammation following myocardial infarction, Circ. Res. 123 (1) (2018) 100–106.
[24] P.B. Devhare, R.B. Ray, Extracellular Vesicles: Novel Mediator for Cell to Cell Communications in Liver Pathogenesis, Mol Aspects Med. 60 (2017) 115–122.
[25] A.I. Masyuk, T.V. Masyuk, N.F. Larusso, Exosomes in the pathogenesis, diagnostics and therapeutics of liver diseases,, J Hepatol. 59 (3) (2013) 621–625.
[26] R. Liu, et al., Cholangiocyte-derived exosomal long noncoding RNA H19 promotes hepatic stellate cell activation and cholestatic liver fibrosis, Hepatology 70 (4) (2019) 1317–1335.
[27] X. Li, et al., Cholangiocyte-derived Exosomal Long Noncoding RNA H19 Promotes Cholestatic Liver Injury in Mouse and Human, Hepatology 68 (2) (2018) 599–615.
[28] L. Chen, et al., Hepatocyte-derived exosomal MiR-194 activates PMVECs and promotes angiogenesis in hepatopulmonary syndrome, Cell Death Dis 10 (11) (2019) 853–870.
[29] Y. Yang, et al., A comparison of two common bile duct ligation methods to establish hepatopulmonary syndrome animal models, Lab. Anim 49 (1) (2015) 71–79.
[30] C. Yang, et al., The Broad Complex isoform 2 (BrC-Z2) transcriptional factor plays a critical role in vitellogenin transcription in the silkworm Bombyx mori, BBA - General Subjects 1840 (9) (2014) 2674–2684.
[31] . Chen CY, et al., Exosomal DMBT1 from human urine-derived stem cells facilitates diabetic wound repair by promoting angiogenesis, Theranostics 8 (6) (2018) 1607–1623.
[32] K.M. Welch-Reardon, N. Wu, C.C.W. Hughes, A role for partial endothelial–mesenchymal transitions in angiogenesis? Arterioscler Thromb Vasc Biol 35 (2) (2015) 303–308.
[33] T.M. Williams, et al., Identification of a zinc finger protein that inhibits IL-2 gene expression, Science 254 (5039) (1991) 1791–1794.
[34] E. Sánchez-Tilló, et al., ZEB1 represses E-cadherin and induces an EMT by recruiting the SWI/SNF chromatin-remodeling protein BRG1, Oncogene 29 (24) (2010) 3490–3500.
[35] M. Kojima, et al., Exosomes, not protein or lipids, in mesenteric lymph activate inflammation: Unlocking the mystery of post-shock multiple organ failure, J Trauma Acute Care Surg 82 (1) (2017) 42–50.
[36] D. Xu, et al., Requirement of miR-9-dependent regulation of Myocd in PASMCs phenotypic modulation and proliferation induced by hepatopulmonary syndrome rat serum, J. Cell Mol. Med. 19 (10) (2015) 2453–2461.
[37] CC Wang, et al., Rosuvastatin Improves Hepatopulmonary Syndrome through Inhibition of Inflammatory Angiogenesis of Lung, Clin Sci 129 (2015) 449–460.
[38] J. Zeng, et al., Effect of annexin A2 on hepatopulmonary syndrome rat serum-induced proliferation of pulmonary arterial smooth muscle cells, Respir Physiol Neurobiol 185 (2) (2013) 332–338.
[39] B. Yi, et al., Annexin A1 protein regulates the expression of PMVEC cytoskeletal proteins in CBDL rat serum-induced pulmonary microvascular remodeling, J. Transl. Med. 11 (1) (2013) 1–8.
[40] B. Yi, et al., cGMP-dependent protein kinase Iα transfection inhibits hypoxia-induced migration, phenotype modulation and annexins A1 expression in human pulmonary artery smooth muscle cells, Biochem Biophys Res Commun 418 (4) (2012) 598–602.
[41] N. Javeed, D. Mukhopadhyay, Exosomes and their role in the micro-/macro-environment: a comprehensive review, J Biomed Res 31 (5) (2017) 386–394.
[42] C. Kilchert, S. Wittmann, L. Vasiljeva, The Regulation and Functions of the Nuclear RNA Exosome Complex, Nat Rev Mol Cell Biol 17 (2016) 227–239.
[43] B. Shashi, et al., Circulating microRNAs in exosomes indicate hepatocyte injury and inflammation in alcoholic, drug-induced, and inflammatory liver diseases, Hepatology 56 (5) (2012).
[44] H. Okada, R. Kalluri, Cellular and Molecular Pathways that Lead to Progression and Regression of Renal Fibrogenesis, Curr Mol Med 5 (5) (2005) 467–474.
[45] H. Okada, R. Kalluri, Recapitulation of kidney development paradigms by BMP-7 reverses chronic renal injury, Clin. Exp. Nephrol. 9 (2) (2005) 100–101.